Preparation of Nanocrystalline High Entropy Alloys via Cryomilling of Cast Ingots

Nirmal Kumar (0000-0001-8795-7857), C.S. Tiwary[2] (0000-0001-9760-9768), Krishanu Biswas*

[1]Department of Materials Science and Engineering, Indian Institute of Technology Kanpur, Kanpur India, 208016, INDIA

[2]Department of Materials Science and Engineering, Indian Institute of Technology Gandhinagar, Gandhinagar - 382355, INDIA

Abstract

The advancement of nanotechnology demands large scale preparation of nanocrystalline powder of innovative materials. High entropy alloys (HEAs) exhibit unique properties; mechanical, thermal, magnetic etc., making them potentials candidates for applications in energy, environment and biomaterials etc. Thus, there is a need to develop novel synthesis methods to prepare nanocrystalline high purity HEAs in large quantity. Conventional mechanical alloying (MA) of the multi component metallic powder mixture requires larger milling time and it is prone to contaminations and phase transformation. The present investigation reports a unique approach, involving casting followed by cryomilling, leading to formation of nanocrystalline HEAs powder, which are relatively contaminations free with narrow size distribution. Using examples of two FCC and one BCC single phase HEAs, it has been shown that large scale nanocrystalline HEAs powder can be prepared after few hours of cryomilling at 123 K. The formation of nanocrystalline HEAs during cryomilling has been discussed using theoretically available approaches.

Keywords: Nanocrystalline, HEAs, Cryomilling, FCC, BCC, TEM

---

*Corresponding author: Email: kbiswas@iitk.ac.in; Phone: +91512-259-6184; Fax: +91512-2597505

1. Introduction

The exploration of novel nanomaterials for various applications in the field of nano-science and nanotechnology has slowly been maturing with discovery of new and advanced materials. It is well known that, the exceptional properties of nano-materials having surface area - to-volume ratio make these materials suitable for various applications [1], such as catalytic[2,3], optical [4,5], anti-bacterial [6,7], magnetic [8], biomedical applications [9] etc. In this regard, alloy nanoparticles found to exhibit exceptional properties for these applications due to the possibility of different combination of element being used. Hence, the alloy nanoparticles possess distinctly different properties from the constituent elements as well as bulk alloys, allowing them to be exploited for various applications. These include Ag/Au bimetallic nanoparticle for cancer detection [10], Sn-Ag-Cu for low temperature lead free inter-connect [11], Fe/Cu nanocrystalline multilayers for soft magnetic application [12]. Furthermore, the properties of the alloy nanoparticles can further be tailored by tuning the number and type of constituent elements, the composition, degree of chemical ordering and morphology. However, continuous advancement in the nanotechnology requires design and development of novel alloy nanoparticles including multi-metallic high entropy alloys [13-19]. Therefore, we require devising novel strategies to prepare these nanoparticles in large quantity.

High entropy alloys are considered as multi-metallic cocktail of at least five elements in equal or near equal proportions and thus termed as concentrated multi-principal element alloys [20,21]. Discovered in 2004, the research activities on these alloys have been vigorous across the globe [22,23,17,24-27]. They exhibit unique set of mechanical (combination of strength, ductility and toughness)[28,29], physical, thermal, magnetic properties due to their intrinsic nature and hence, are deemed to be potential candidates for applications in energy, biomedical, catalysis sectors

[30-34]. However, preparation of nanocrystalline HEA in large quality is a challenge to the material science community.

Conventionally, nanocrystalline HEAs powder has been prepared using mechanical alloying of the elemental mixture. There exist two experimental pathways to obtain nanocrystalline HEAs *via* ball milling [35,36,16]. First, individual powders of required elements are fed into a ball mill and milled sufficiently long until HEA phases form. This pathway is known as mechanical alloying (MA). Second approach is related to crushing of the HEA ingot conventionally cast *via* ball milling at extremely low temperature. In the first case, NPs of HEAs may form but it requires longer milling time, which can impart unwanted impurity or contamination from the milling tools as well as atmospheric oxygen and nitrogen. The multicomponent HEAs are prone to oxidation and hence pure nanocrystalline HEAs are difficult to achieve *via* conventional ball milling route. Being multicomponent, the HEA NPs, obtained *via* mechanical alloying of individual powder mixture may lead to formation of metastable phases [37-39]. On the other hand, the second route, *i.e*, casting followed by cryomilling, requires the material to be hard and brittle at low temperature. The consideration of high ductility (>40%) and toughness (>250 $MPa.m^{1/2}$) of FCC HEA phases from high to low temperature (800 to -196°C) makes the formation of NPs of HEA *via* cryomilling difficult. The high ductility and toughness lead to easier cold welding, which is considered an obstacle to the formation of NPs *via* cryomilling[40]. However, cryomilling has many advantages, including low contamination, reduced oxidation, suppression of recovery and recrystallization etc [41-45]. Therefore, if successful, cryomilling is expected to deliver the solution to synthesize of nanocrystalline HEAs in large quantity, useful for variety of applications [46].

In the present investigation paper we demonstrate an easily scalable, cryomilling technique to prepare high entropy alloys nanoparticles (HEAs-NPs) in large quantity. We have selected three alloy compositions; two are single phase FCC high entropy alloys ($Fe_{0.2}Cr_{0.2}Mn_{0.2}Ni_{0.2}Co_{0.2}$), ($Cu_{0.2}Ag_{0.2}Au_{0.2}Pt_{0.2}Pd_{0.2}$) and third one is a single phase BCC high entropy alloy ($Fe_{0.2}Cr_{0.2}Mn_{0.2}V_{0.2}Al_{0.2}$). FCC are relatively more ductile and tough and hence, more difficult to crush to form HEA-NPs. In each case, alloys nanoparticles have been prepared and characterized using X-ray diffraction (XRD), transmission electron microscope (TEM), surface plasmon resonance. The mechanism of the formation of HEAs-NPs has also been discussed in detail.

2. Experimental

2.1 Preparation of HEAs

The three different of high entropy alloys ($Cu_{0.2}Ag_{0.2}Au_{0.2}Pt_{0.2}Pd_{0.2}$), ($Fe_{0.2}Cr_{0.2}Mn_{0.2}Ni_{0.2}Co_{0.2}$) and ($Fe_{0.2}Cr_{0.2}Mn_{0.2}V_{0.2}Al_{0.2}$) were prepared using arc melting under high purity argon atmosphere and purity of the pure elements were 99.9 at%, (Alfa Aesar, USA). Utilizing this technique, the bulk ingot of single phase FCC ($Fe_{0.2}Cr_{0.2}Mn_{0.2}Ni_{0.2}Co_{0.2}$), ($Cu_{0.2}Ag_{0.2}Au_{0.2}Pt_{0.2}Pd_{0.2}$) and BCC ($Fe_{0.2}Cr_{0.2}Mn_{0.2}V_{0.2}Al_{0.2}$) HEAs were obtained. The alloys were further homogenized at 1000^{o}C for 10 hours casting to obtain large grains with chemical homogeneity.

2.2 **Preparation of HEAs-NPs**

The HEA ingots have been parted in smaller pieces utilizing diamond saw (Bueheler, USA). Further, these pieces were milled in a custom built cryomill [47] at-160±10^{o}C.The single ball cryomill (schematic is shown in **Figure 1**) was cooled using liquid nitrogen (LN_2). The detailed design and working principle of cryomill ware reported elsewhere [47]. The cryomill is a

vibratory mill having a single ball with diameter 5 cm and vial 9.5 cm with volume of 250 cc. Thus, ball amplitude 2 mm was maintained through milling using tungsten carbide (WC) ball-vial. The milling chamber was continuously purged using argon (Ar) gas to protect the powder from oxidation during milling. After six hours of cryomilling, the HEAs-NPs were collected for characterization.

2.3. Characterization of HEA-NPs

The X-ray diffractometer (PanalyticalXPert make PANalytical) was used with Cu K_α radiation (λ=1.54056 nm) to study the phases in the bulk as well as cryo-milled powder. The annealed strain free Si powder was used to determine instrumental broadening for crystallite size measurement. The small quantity of nanocrystalline powder was dispersed in ultrapure methanol (CH_3OH) using sonication. The few drops of the prepared solution was placed over carbon coated copper (Cu) grid and dried 10 hours prior to TEM measurements. The transmission electron microscope (FEI, Technai, G^2 UT- 20, 200 kV, Netherlands) has been used to size analysis. The surface plasmon (characteristics phenomenon of NPs) characteristics was carried out using UV-visible spectroscopy (Thermo scientific, UK). The composition of the as cast and cryomill powders were estimated using electron probe micro analyzer (EPMA- JXA-8230; JEOL, Japan). The quantitative analyses were performed at 25 kV using four types of X-ray detectors: Lithium fluoride (LiFH) crystals; Layered dispersion element (LDE); Pentaerythritol (PET); Thallium acid phthalate (TAP)

3. Results

3.1 X-ray diffraction analysis

The formation of single phase HEA –NPs has been analyzed using X-ray diffraction (XRD), analyses as shown in **Figure 2(a-c)**. The as cast and homogenized alloys, $Fe_{0.2}Cr_{0.2}Mn_{0.2}Ni_{0.2}Co_{0.2}$ (Cantor alloy[48]) and ($Cu_{0.2}Ag_{0.2}Au_{0.2}Pt_{0.2}Pd_{0.2}$) are single phase FCC (face centered cubic) whereas $Fe_{0.2}Cr_{0.2}Mn_{0.2}V_{0.2}Al_{0.2}$alloy is a single phase BCC (body centered cubic). The phase formation has also been investigated after cryomilling of the HEAs ingot (bulk). It has been observed that there is no phase change in the HEAs –NPs post cryomilling. As compared to the ingots, XRD patterns of the nanocrystalline powder show the broadening of the peaks, shown as inset in each case. The broadening of the peaks is primarily due to nanocrystalline nature as well as cold working (lattice strain accumulation) as shown each **Figure (a-c) inset**. Using Hall- Williamson and Scherer analysis [49], the crystallite size as well as lattice have been estimated. The measurements are reported in **Table 1**. However, there is large difference in the crystallite size estimated using TEM and XRD. The powder prepared by cryomilling is expected to produce nanocrystals having irregular shape. In the present case, the crystallite size of different HEA nanoparticles has been estimated using average value of the K[50]. In addition, crystallite size has been estimated by direct measurement using TEM images. However, there is large difference in the crystallite size estimated using TEM and XRD. There are several reasons for this discrepancy.

1. The shape parameter the crystallite size can from crystallite to crystallite due to irregular shape.
2. The HEAs subjected to intrinsic lattice distortion as well as different atomic sizes (all 5 elements), which is might be a reason of abnormal peak broadening causes large difference in crystallite size compared to other techniques [20]. However, the high

entropy alloys have very distorted lattices and different atom sizes, which are the reasons to contribution in broadening.

3. In case of nanoparticles preparation by top down method, the broadening in the XRD peaks contributed from other sources (dislocation density, stacking fault or defects generated by cold work in the crystal system).

3.2 Size and morphology

The size, shape and morphology of the HEAs-NPs have been studied using transmission electron microscope (TEM) to decipher the nature of the cryomilled HEA powder. **Figures 3 (a-b)** show the typical bright field image of $Fe_{0.2}Cr_{0.2}Mn_{0.2}Ni_{0.2}Co_{0.2}$ alloys nanoparticles. **Figure 3b** is the low magnification micrograph revealing distribution of the cryomilled HEA-NPs. The higher magnification bright field (**Fig. 3a**) and dark field image **(Fig. 3(c))** show the irregularly shaped NPs having size ranging from 5- 10 nm. **Table 1** shows the average crystallite size measured using TEM images. **Fig. 3(e)** shows bright field image of particles, where oleylamine has been used as capping agent during dispersion of the nanoparticle prior to the sample preparation for TEM investigation to estimate size of large number of the NPs (~ 500 particles). The histogram has been generated as shown in **Fig. 3d**. The average size is found to be 4±1 nm. The selected area diffraction patterns (SADP) clearly reveals the single-phase FCC HEAs**.** Detailed analysis indicates that the SADP pattern is similar to XRD patterns (**Fig. 2(a)).** Similarly, the bright field TEM image of $Cu_{0.2}Ag_{0.2}Au_{0.2}Pt_{0.2}Pd_{0.2}$ alloys nanoparticles is shown in **Figure 4(a-b)** indicating the average crystallite size 9±5 nm (distribution is shown in **Figure 4d**).The XRD and SADP(**Figure 4(e))** indicate that this is also single phase FCC. The as cast, BCC HEA and the

HEA-NPs has also been investigated using TEM and found to be single phase with average crystallite size of nanoparticles to be 6±2 nm as shown in **Figure 5(a-e)**.

3.3 Compositional measurements

The compositions of ingot and cryomilled powder have been estimated using Electron Probe Micro-Analyzer (EPMA) based Wavelength dispersive spectroscopy (WDS) and Energy dispersive spectroscopy (EDS). The qualitative WDS spectra has shown in **Figure 6.** The qualitative analyses of the spectra clearly indicate that oxygen is only impurity present in the sample and clearly reveal the absence of N. It is to be noted here the carbon arises from the carbon tape as well as resins utilized for mounting the samples during EMPA analysis.

In addition, quantitative analyses of the composition of the ingot and powder have been carried out using EPMA. The results are shown in **Table 2**.The analyses reveal the oxygen concentration is low (varying between 1.98±0.3 to 1.17±0.2 atom% in the bulk alloy and 1.25±0.4 to 0.34±0.4 atom% in the nano powder). It is evident, oxygen content in the powder is significantly lower

3.4 Surface plasmon resonance

The past groundbreaking research on biosensors for detection of single viruses, interaction between different bio-molecules shows that metallic nanoparticles are highly sensitive to optical method using SPR technique [51]. Therefore, the HEA -NPs containing multiple metallic elements could be a promising candidate for the devices required plasmonic as well as magnetic properties[52]. It is to be noted that the nanoparticles show surface plasmon resonance (SPR) band and which is results of electrons collective oscillation [53]. The dielectric of the surrounding medium can have major effect on peak position and intensity[54]. In addition, the shape and size also affect the peak position. As size decreases the SPR resonance band exhibit

blue shift (blue shift: peak shift to lower wavelength and red shift: peak shift to higher wavelength). Hence, surface plasmon resonance occurs in nanostructured materials the position of the SPR peaks are debatable in the literature due to the fact that peaks positions affected by several parameters indicating- dielectric of surrounding, refractive index of solvent, shape, size and distribution of nanoparticles etc. The Cantor alloy ($Fe_{0.2}Cr_{0.2}Mn_{0.2}Ni_{0.2}Co_{0.2}$) NPs have shown two SPR bands at λ_{max} = 239, 293 nm and $Cu_{0.2}Ag_{0.2}Au_{0.2}Pt_{0.2}Pd_{0.2}$ alloy NPs have shown two peak at 279 and 284 nm. Similarly, $Fe_{0.2}Cr_{0.2}Mn_{0.2}V_{0.2}Al_{0.2}$ NPs revealed the SPR band at λ_{max} = 354 nm **Figure 7(a)**. There is no literature available on the surface plasmon study of HEAs-NPs. Hence, it is not possible to discuss the peak position for HEA-NPs. In addition, the HEAs-NP dispersions is measured quite stable in methanol as shown in **Figure 7(b)** which might be due to nanocrystalline nature and electrostatic stabilization [55,56] of the NPs in methanol.

4. Discussion

The results of the present investigation categorically show that HEAs-NPs can be prepared using cryomilling of the cast ingots, which are relatively ductile and toughness. These NPs retain crystals structure of the phases in the bulk ingot. The detailed TEM measurements reveal narrow size distribution of HEA-NPs. Further, we shall explain the mechanisms of formation of nanocrystalline HEA via cryomilling.

It is to be noted that cryo-milling is a type of milling in which, powder particles are crushed/milled at temperature below 123K. It suppresses the recrystallization, dynamic recovery, processes leading to refinement of the grain and formation of nanocrystalline materials in short period of time. Accordingly, it reduces the milling duration and hence suppresses the contamination or milling media debris from the milling tools and atmosphere. Thus, cryomilling

takes advantage of the extremely low temperature (boiling temperature 77 K) of the liquid nitrogen (cooling media) as well as those related with room temperature ball milling. Cooling of the ball-vial and milling powders is an efficient way to increase the fracturing process, leading to a nano-grained structures and early grain refinement. In addition, the powder coarsening (cold bond) and coating (sticking) to the milling media can effectively be suppressed leading to more efficient product outcome like higher yield and powder particles refinement. The milling with argon atmosphere and extremely low temperature reduce the oxidation of the powder.

Because the formation of nanoparticles using room temperature milling is requires very long time of milling, it can easily impart unavoidable contamination from the milling tools [57]. In case of highly ductile and tough materials (HEA), it is required to be milled for very long time to obtain nanoparticle via ball milling at room temperature. Therefore, the contaminations are mixed to milling powder atomically and hence it might alter the crystal structure as well multi-atomic pre-calculated proportion. Therefore, the extremely low temperature during cryomilling helps in many ways [58,59]. In the following, we should discuss the various advantages of cryomilling process, leading to formation of nanocrystalline. **Table 3** shows mechanical properties of the HEA alloys; i.e. FCC $Fe_{0.2}Cr_{0.2}Mn_{0.2}Ni_{0.2}Co_{0.2}$ and BCC $Fe_{0.2}Cr_{0.2}Mn_{0.2}V_{0.2}Al_{0.2}$ [17, 53]. To the best of the authors' knowledge, mechanical property of $Cu_{0.2}Ag_{0.2}Au_{0.2}Pt_{0.2}Pd_{0.2}$ is not available in the literature. The HEAs phases exhibit high ductility and toughness even at LN_2 temperature and thus making it difficult to suppress the deformation and accelerate the fracturing process.

According to Fecht et al. grain refinement *via* mechanical milling process occurs in five stages [40]: (i) flattening, (ii) cold welding, (iii) fracturing, (iv) equiaxed particles formation followed by random welding and (v) steady state particle formation. In the initial stage, severe plastic

deformation is effectively applied to the particles, which is lead to the creation of the shear bands due to localized severe deformation. The deformation generally accumulates high density of localized dislocation tangled networks, resulting in the increase of plastic strain. Further, the second stage involves formation of sub-grains separated by low-angle grain boundaries. In the third stage, repeated deformation of the particles creates additional shear bands with further fracturing of the sheets of particles formed due to random cold welding. In the last stage, a steady state is reached between cold welding and fracturing. Therefore, the phenomenon of cold welding is extensively observed during ball milling of the ductile metallic material including HEAs. This can be vigorously suppressed by reducing temperature (cryomilling). Therefore, the mechanical milling extremely low temperature can effectively shorten five-stage process to three stage process, flattening of particles (sheet formation), fracturing of sheets and steady state nano-particle formation as shown in Figure 8. It might be possible that the flattened powder particles are slightly cold welded but that bond strength of the cold welds is very low, which is easily breakable during further cryomilling. In addition, the low temperature reduces the dynamic recovery in HEAs [60,61], which can accelerate the fracturing of particles. In addition, the extremely low temperature reduces the rate of oxidation [62], which is beneficial to protect the nano-crystals from oxidation during milling.

The formation of HEAs by casting and pulverized them into nanoparticles by cryomilling is the easiest way to synthesized HEAs-NPs, which is capable to prepare large scale nanomaterials. The cryomilling is advantageous due to short time of milling to form nanoparticles as it vigorously reduces debris from milling tools [47,56,63]. Secondly, this process can be utilized to prepare HEA-NPs in large quantity. In order to estimation of the quantity of HEA- NPs, the equation 1 has been used [47,64].

Percent Yield = (Weight of nanoparticles / total weight of milling powder) ×100 (1)

Earlier study shows that the yield of the process is about 97% with only 3% approximately of the milled powder is lost due to coating on the ball and vials. The present cryomill [47] having 250 cc vial and 150 cc ball can mill maximum 25 g at a time i.e. is with ball to powder ratio of 40:1. It requires 6 hours to synthesize NPs having size less than 10 nm. Thus, it is possible to obtain about 97 g HEA-NPs/day. This amount is substantially large as compared to available green synthesis techniques such as wet chemical synthesis, pulsed discharge arc discharge, plasma induced chemical synthesis or even conventional mechanical alloying. The detailed literature survey reveals that yield of the similar process (**commination or arc dressing during minerals beneficiation**) is about 90% for industrial scales of production several tones. Hence the yield is true for industrial scale.

Conclusion

The present investigation demonstrates the large scale preparation of HEAs-NPs successfully by cryomilling bulk high entropy alloy ingots. In general, the following conclusions can be made

i) the cryomilling can prepare HEAs-NPs less than10 nm size with high yield
ii) it allows retaining equiatomic proportion of composition of HEAs.
iii) Cryomilling imparts negligible contamination from milling tools and atmosphere.
iv) the bulk HEAs and nanoparticles HEAs are retain their crystal structure in cryomilling
v) large scale preparation of HEA-NPs can be achieved by cryomilling.

Acknowledgement

The authors wish to thank SERB-DST for their financial support to carry out this work and wish to thank Advanced Center for Materials Science, Indian Institute of Technology Kanpur for utilizing X-ray diffraction facility.

References

[1] Sattler KD. Handbook of Nanophysics: Nanotubes and Nanowires. CRC Press, 2010

[2] Liu X, Sui Y, Yang X, Wei Y, Zou B. Cu Nanowires with Clean Surfaces: Synthesis and Enhanced Electrocatalytic Activity. ACS Appl Mater Interfaces 2016; 8 (40):26886-26894.

[3] Xu Y, Lin X. Facile fabrication and electrocatalytic activity of Pt0.9Pd0.1 alloy film catalysts. J Power Sources 2007; 170 (1):13-19.

[4] Huang X, El-Sayed MA. Gold nanoparticles: Optical properties and implementations in cancer diagnosis and photothermal therapy. J Adv Res 2010; 1 (1):13-28.

[5] Li XD, Chen TP, Liu Y, Leong KC. Influence of localized surface plasmon resonance and free electrons on the optical properties of ultrathin Au films: A study of the aggregation effect. Opt Express 2014; 22 (5):5124-5132.

[6] Tsai T-T, Huang T-H, Chang C-J, Yi-Ju Ho N, Tseng Y-T, Chen C-F. Antibacterial cellulose paper made with silver-coated gold nanoparticles. Scientific Reports 2017; 7 (1):3155.

[7] Cloutier M, Mantovani D, Rosei F. Antibacterial Coatings: Challenges, Perspectives, and Opportunities. Trends Biotechnol 2015; 33 (11):637-652.

[8] Yang H-W, Chung C-M, Ding JY. Effect of Ni doping on the structural and magnetic properties of FePt nanoparticles. J Magn Magn Mater 2007; 312 (1):239-244.

[9] Travan A, Marsich E, Donati I, Paoletti S (2007) Silver Nanocomposites and Their Biomedical Applications. In: Nanotechnologies for the Life Sciences. Wiley-VCH Verlag GmbH & Co. KGaA. doi:10.1002/9783527610419.ntls0219

[10] Patskovsky S, Bergeron E, Rioux D, Simard M, Meunier M. Hyperspectral reflected light microscopy of plasmonic Au/Ag alloy nanoparticles incubated as multiplex chromatic biomarkers with cancer cells. Analyst 2014; 139 (20):5247-5253.

[11] Jiang H, Moon KS, Wong CP Tin/silver/copper alloy nanoparticle pastes for low temperature lead-free interconnect applications. In: Proceedings - Electronic Components and Technology Conference, 2008. pp 1400-1404. doi:10.1109/ectc.2008.4550160

[12] Naoe M, Matsumiya H, Ichihara T, Nakagawa S. Preparation of soft magnetic films of nanocrystalline Fe-Cu-Nb-Si-B alloy by facing targets sputtering. J Appl Phys 1998; 83 (11):6673-6675.

[13] Cantor B. Multicomponent and high entropy alloys. Entropy 2014; 16 (9):4749-4768.

[14] Sumanta Samal SM, Ajit Kumar Misra, Krishanu Biswas, B. Govind. Mechanical Properties of Novel Ti-Cu-Ni-Co-Fe High Entropy Alloys. Mater Sci Forum 2014; 790-791:503-508.

[15] Mohanty S, Samal S, Tazuddin A, Twari C, Gurao N, Biswas K. Effect of processing route on phase stability in equiatomic multicomponent Ti20Fe20Ni20Co20Cu20 high entropy alloy. Mater Sci Tech 2015; 31:10.

[16] Mohanty S, Gurao NP, Biswas K. Sinter ageing of equiatomic Al20Co20Cu20Zn20Ni20 high entropy alloy via mechanical alloying. Mater Sci Eng A 2014; 617:211-218.

[17] Yeh JW. Recent progress in high-entropy alloys. Ann Chim - Sci Mat 2006; 31 (6):633-648.

[18] Tsai KY, Tsai MH, Yeh JW. Sluggish diffusion in Co-Cr-Fe-Mn-Ni high-entropy alloys. Acta mater 2013; 61 (13):4887-4897.

[19] Mishra A, Samal S, Biswas K. Solidification Behaviour of Ti–Cu–Fe–Co–Ni High Entropy Alloys. Trans Indian Inst Met 2012; 65 (6):725-730.

[20] Murty BS, Yeh JW, Ranganathan S (2014) Chapter 2 - High-Entropy Alloys: Basic Concepts. In: High Entropy Alloys. Butterworth-Heinemann, Boston, pp 13-35. doi:10.1016/B978-0-12-800251-3.00002-X

[21] Zhou Y, Zhou D, Jin X, Zhang L, Du X, Li B. Design of non-equiatomic medium-entropy alloys. Scientific Reports 2018; 8 (1):1.

[22] Murty BS, Yeh JW, Ranganathan S (2014) Chapter 1 - A Brief History of Alloys and the Birth of High-Entropy Alloys. In: High Entropy Alloys. Butterworth-Heinemann, Boston, pp 1-12. doi:10.1016/B978-0-12-800251-3.00001-8

[23] Miracle DB, Senkov ON. A critical review of high entropy alloys and related concepts. Acta mater 2017; 122 (Supplement C):448-511.

[24] Pickering EJ, Jones NG. High-entropy alloys: a critical assessment of their founding principles and future prospects. Int Mater Rev 2016; 61 (3):183-202.

[25] Gao MC, Yeh JW, Liaw PK, Zhang Y. High-entropy Alloys: Fundamentals and Applications. Springer, 2016

[26] Zhang W, Liaw PK, Zhang Y. Science and technology in high-entropy alloys. Science China Materials 2018; 61 (1):2-22.

[27] Li RX, Liaw PK, Zhang Y. Synthesis of AlxCoCrFeNi high-entropy alloys by high-gravity combustion from oxides. Mater Sci Eng A 2017; 707:668-673.

[28] Otto F, Dlouhý A, Somsen C, Bei H, Eggeler G, George EP. The influences of temperature and microstructure on the tensile properties of a CoCrFeMnNi high-entropy alloy. Acta mater 2013; 61 (15):5743-5755.

[29] Gludovatz B, Hohenwarter A, Catoor D, Chang EH, George EP, Ritchie RO. A fracture-resistant high-entropy alloy for cryogenic applications. Science 2014; 345 (6201):1153-1158.

[30] Na SM, Yoo JH, Lambert PK, Jones NJ. Room-temperature ferromagnetic transitions and the temperature dependence of magnetic behaviors in FeCoNiCr-based high-entropy alloys. AIP Advances 2018; 8 (5)

[31] Huo W, Liu X, Tan S, Fang F, Xie Z, Shang J, Jiang J. Ultrahigh hardness and high electrical resistivity in nano-twinned, nanocrystalline high-entropy alloy films. Appl Surf Sci 2018; 439:222-225.

[32] Praveen S, Kim HS. High-Entropy Alloys: Potential Candidates for High-Temperature Applications – An Overview. Adv Eng Mater 2018; 20 (1)

[33] Kumar A, Gupta M. An insight into evolution of light weight high entropy alloys: A review. Metals 2016; 6 (9)

[34] Ye YF, Wang Q, Lu J, Liu CT, Yang Y. High-entropy alloy: challenges and prospects. Materials Today 2016; 19 (6):349-362.

[35] Zhang Y, Zhang B, Li K, Zhao G-L, Guo SM. Electromagnetic interference shielding effectiveness of high entropy AlCoCrFeNi alloy powder laden composites. J Alloys Compd 2018; 734:220-228.

[36] Yadav S, Kumar A, Biswas K. Wear behavior of high entropy alloys containing soft dispersoids (Pb, Bi). Mater Chem Phys 2017;

[37] Vaidya M, Prasad A, Parakh A, Murty BS. Influence of sequence of elemental addition on phase evolution in nanocrystalline AlCoCrFeNi: Novel approach to alloy synthesis using mechanical alloying. Mater Des 2017; 126:37-46.

[38] Biswas K, Phanikumar G, Chattopadhyay K, Volkmann T, Funke O, Holland-Moritz D, Herlach DM. Rapid solidification behaviour of undercooled levitated Fe–Ge alloy droplets. Mater Sci Eng A 2004; 375-377 (Supplement C):464-467.

[39] Biswas K, Phanikumar G, Holland-Moritz D, Herlach DM, Chattopadhyay K. Disorder trapping and grain refinement during solidification of undercooled Fe–18 at% Ge melts. Philosophical Magazine 2007; 87 (25):3817-3837.

[40] Fecht HJ. Nanostructure formation by mechanical attrition. Nanostruct Mater 1995; 6 (1–4):33-42.

[41] Verma A, Biswas K, Tiwary C, Mondal A, Chattopadhyay K. Combined Cryo and Room-Temperature Ball Milling to Produce Ultrafine Halide Crystallites. Metall Mater Trans A 2011; 42 (4):1127-1137.

[42] Tiwary C, Verma A, Kashyp S, Biswas K, Chattopadhyay K. Preparation of Freestanding Zn Nanocrystallites by Combined Milling at Cryogenic and Room Temperatures. Metall Mater Trans A 2013; 44 (4):1917-1924.

[43] Tiwary CS, Verma A, Biswas K, Mondal AK, Chattopadhyay K. Preparation of ultrafine CsCl crystallites by combined cryogenic and room temperature ball milling. Ceram Int 2011; 37 (8):3677-3686.

[44] Barai K, Tiwary CS, Chattopadhyay PP, Chattopadhyay K. Synthesis of free standing nanocrystalline Cu by ball milling at cryogenic temperature. Mater Sci Eng A 2012; 558 (0):52-58.

[45] Tiwary CS, Kashyap S, Biswas K, Chattopadhyay K. Synthesis of pure iron magnetic nanoparticles in large quantity. J Phys D: Appl Phys 2013; 46 (38):385001-385005.

[46] Murty BS, Yeh JW, Ranganathan S (2014) Chapter 10 - Applications and Future Directions. In: High Entropy Alloys. Butterworth-Heinemann, Boston, pp 159-169. doi:10.1016/B978-0-12-800251-3.00010-9

[47] Kumar N, Biswas K. Fabrication of novel cryomill for synthesis of high purity metallic nanoparticles. Rev Sci Instrum 2015; 86 (8):083903-083908.

[48] Cantor B, Chang ITH, Knight P, Vincent AJB. Microstructural development in equiatomic multicomponent alloys. Mater Sci Eng A 2004; 375-377 (1-2 SPEC. ISS.):213-218.

[49] Williamson GK, Hall WH. X-ray line broadening from filed aluminium and wolfram. Acta Metallurgica 1953; 1 (1):22-31.

[50] Langford JI, Wilson AJC. Scherrer after sixty years: A survey and some new results in the determination of crystallite size. Journal of Applied Crystallography 1978; 11 (2):102-113.

[51] Shpacovitch V. Application of Surface Plasmon Resonance (SPR) for the Detection of Single Viruses and Single Biological Nano-objects. Journal of Bacteriology and Parasitology 2012; 3 (7)

[52] Messina GC, Sinatra MG, Bonanni V, Brescia R, Alabastri A, Pineider F, Campo G, Sangregorio C, Li-Destri G, Sfuncia G, Marletta G, Condorelli M, Proietti Zaccaria R, De Angelis F, Compagnini G. Tuning the Composition of Alloy Nanoparticles Through Laser Mixing: The Role of Surface Plasmon Resonance. J Phys Chem C 2016; 120 (23):12810-12818.

[53] Linic S, Aslam U, Boerigter C, Morabito M. Photochemical transformations on plasmonic metal nanoparticles. Nat Mater 2015; 14 (6):567-576.

[54] Rak MJ, Friscic T, Moores A. One-step, solvent-free mechanosynthesis of silver nanoparticle-infused lignin composites for use as highly active multidrug resistant antibacterial filters. RSC Advances 2016; 6 (63):58365-58370.

[55] Bell GM, Levine S. The electrostrictive effect in diffuse charged layers. J Colloid Interface Sci 1976; 56 (2):218-226.

[56] Kumar N, Biswas K, Gupta RK. Green synthesis of Ag nanoparticles in large quantity by cryomilling. RSC Advances 2016; 6 (112):111380-111388.

[57] Goujon C, Goeuriot P, Delcroix P, Le Caër G. Mechanical alloying during cryomilling of a 5000 Al alloy/AlN powder: the effect of contamination. J Alloys Compd 2001; 315 (1–2):276-283.

[58] Blewitt TH, Coltman RR, Redman JK. Low-Temperature Deformation of Copper Single Crystals. J Appl Phys 1957; 28 (6):651-660.

[59] Wigley DA. Mechanical properties of materials at low temperatures. Cryogenics 1968; 8 (1):3-12.

[60] Hallén H. A theory of dynamic recovery in F.C.C. metals. Mater Sci Eng 1985; 72 (2):119-123.

[61] Sharma P, Biswas K, Mondal AK, Chattopadhyay K. Size effect on the lattice parameter of KCl during mechanical milling. Scripta Materialia 2009; 61 (6):600-603.

[62] Rhodin TN. Low Temperature Oxidation of Copper. I. Physical Mechanism. J Am Chem Soc 1950; 72 (11):5102-5106.

[63] Kumar N, Biswas K. Cryomilling: An environment friendly approach of preparation large quantity ultra refined pure aluminium nanoparticles. J Mater Res Technol 2017;

[64] Deepika A, Li LH, Glushenkov AM, Hait SK, Hodgson P, Chen Y. High-efficient production of boron nitride nanosheets via an optimized ball milling process for lubrication in oil. Scientific Reports 2014; 4

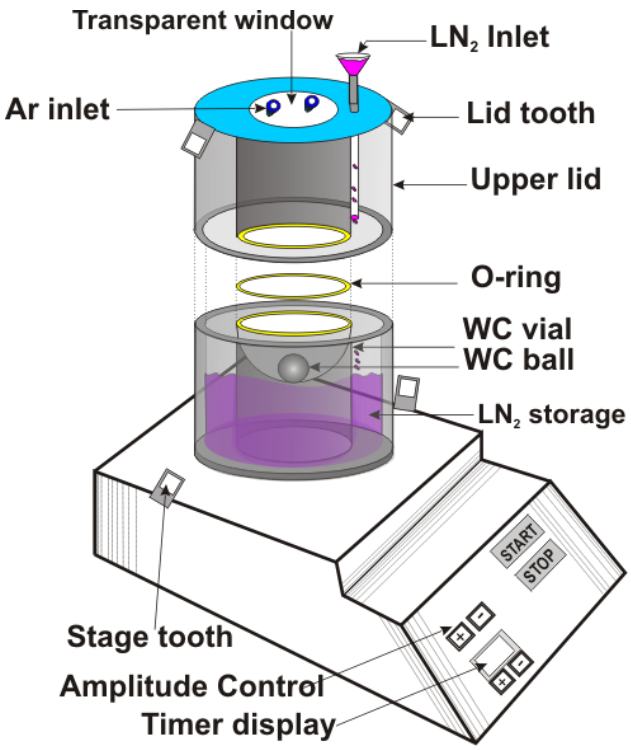

Figure1: Schematic of custom built single ball cryomill (WC-Tungsten carbide)

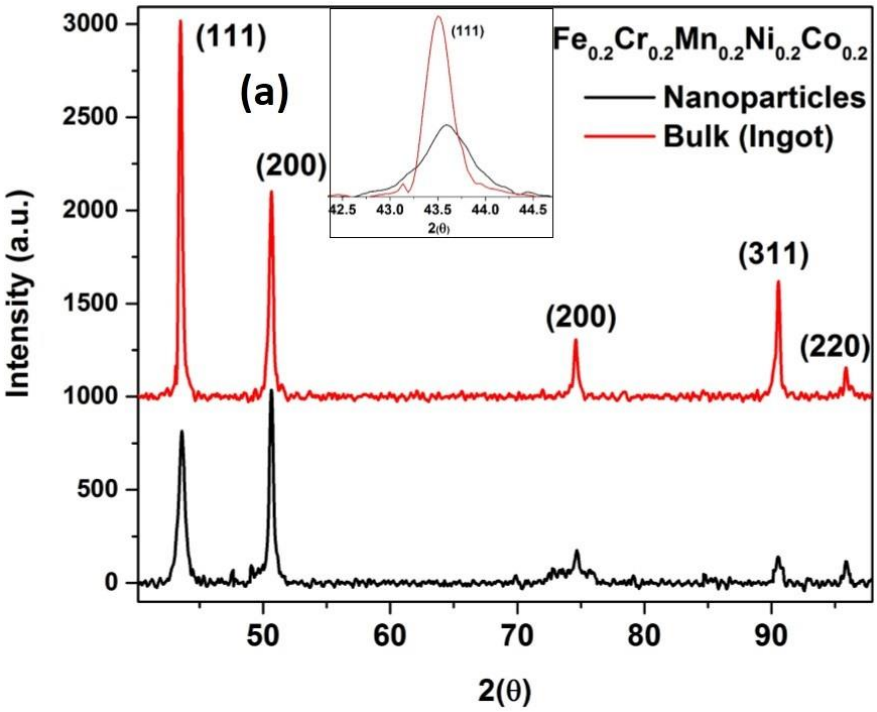
(a)
(111)
(200)
(200)
(311)
(220)
(111)
42.5
43.0
43.5
44.0
44.5
2(θ)
Fe0.2Cr0.2Mn0.2Ni0.2Co0.2
Nanoparticles
Bulk (Ingot)
Intensity (a.u.)
3000
2500
2000
1500
1000
500
0
50
60
70
80
90
2(θ)

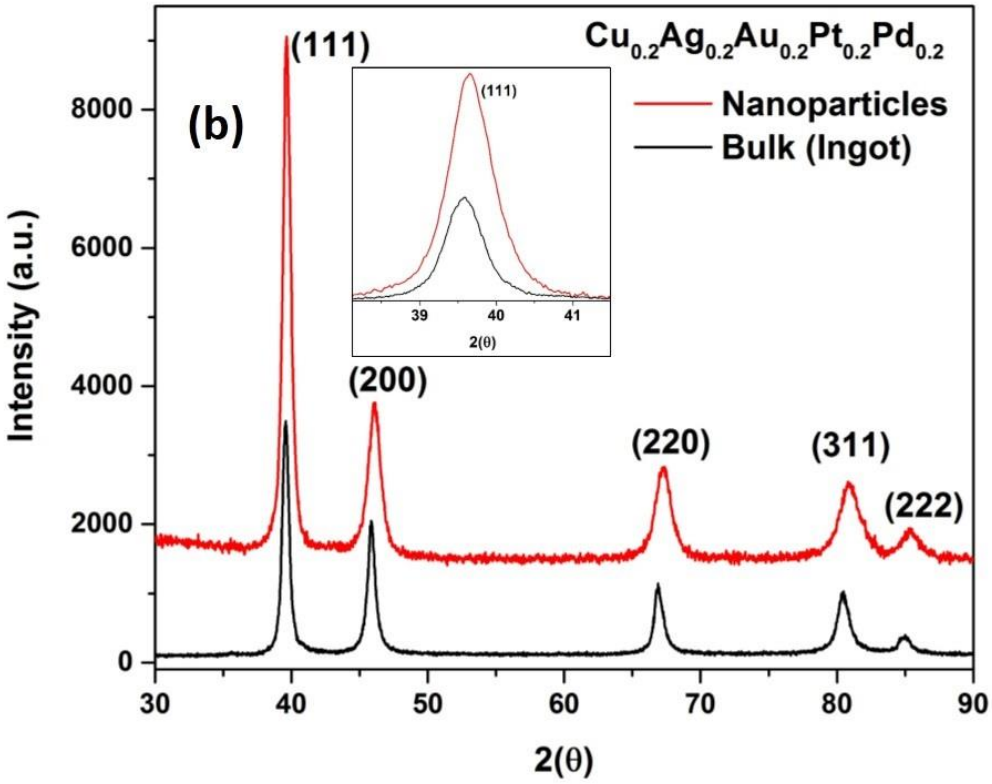
(b)
(111)
(200)
(220)
(311)
(222)
(111)
39
40
41
2(θ)
Cu0.2Ag0.2Au0.2Pt0.2Pd0.2
Nanoparticles
Bulk (Ingot)
Intensity (a.u.)
8000
6000
4000
2000
0
30
40
50
60
70
80
90
2(θ)

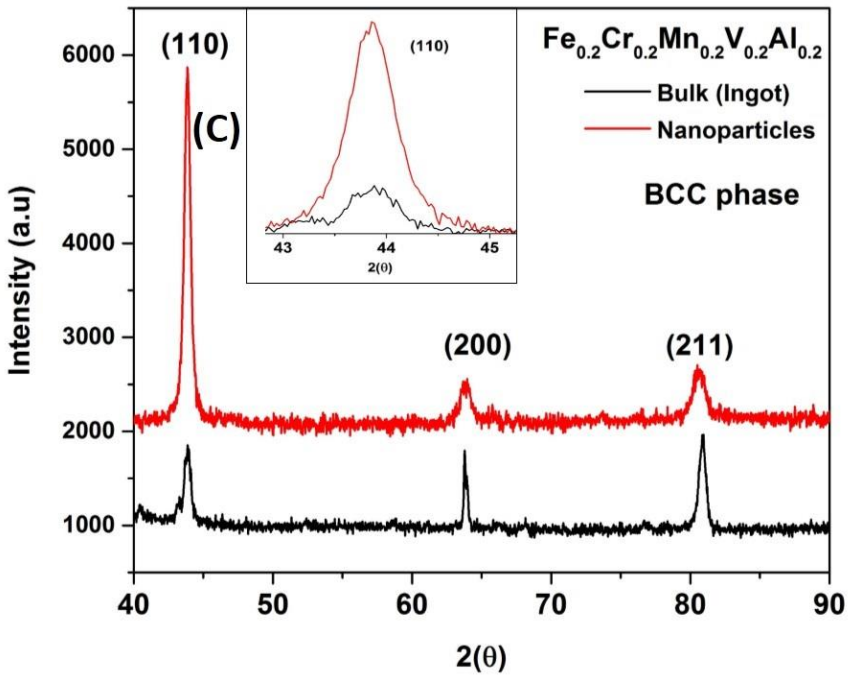

Figure 2: X-ray diffraction pattern of HEAs ingot along with nanoparticles; **(a)** single phase FCC ($Fe_{0.2}Cr_{0.2}Mn_{0.2}Ni_{0.2}Co_{0.2}$); **(b)** single phase FCC ($Cu_{0.2}Ag_{0.2}Au_{0.2}Pt_{0.2}Pd_{0.2}$); **(c)** single phase BCC ($Fe_{0.2}Cr_{0.2}Mn_{0.2}V_{0.2}Al_{0.2}$), Inset shown the broadening effect of (111) and (110) peaks of FCC and BCC respectively. The intensity ratio peak inset image (a) 2.5; image inset (b) 2.1; image inset (c) 2.

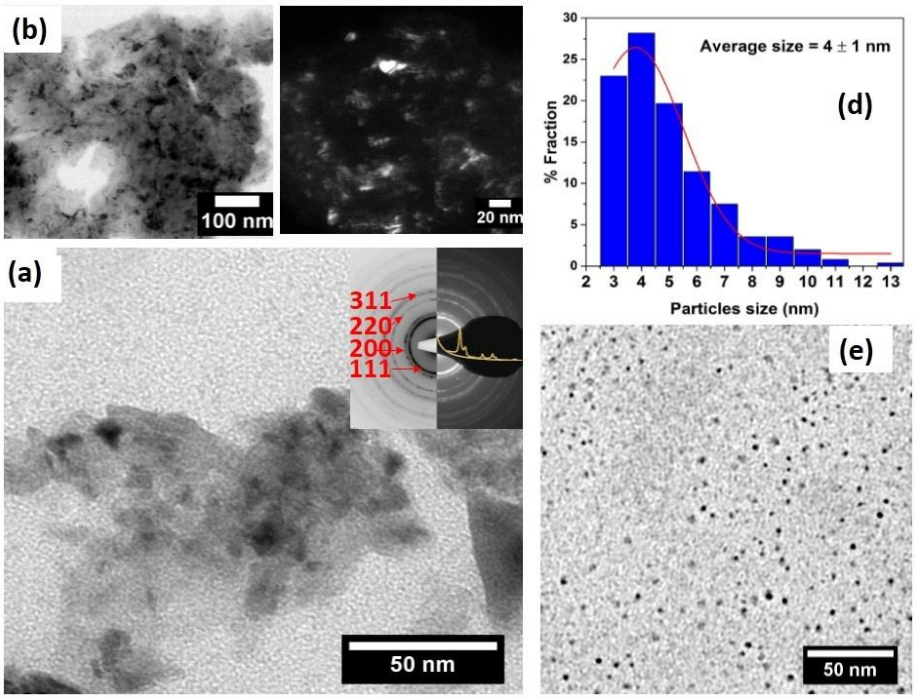

Figure3: (a-b) TEM bright field image of HEAs –NPs ($Fe_{0.2}Cr_{0.2}Mn_{0.2}Ni_{0.2}Co_0$); inset showed selected area diffraction; **(c)** dark filed mage of nanoparticles; **(d)** distribution of HEA-NPs; **(e)**bright field image of nanoparticles stabilized using capping agentOleylamine.

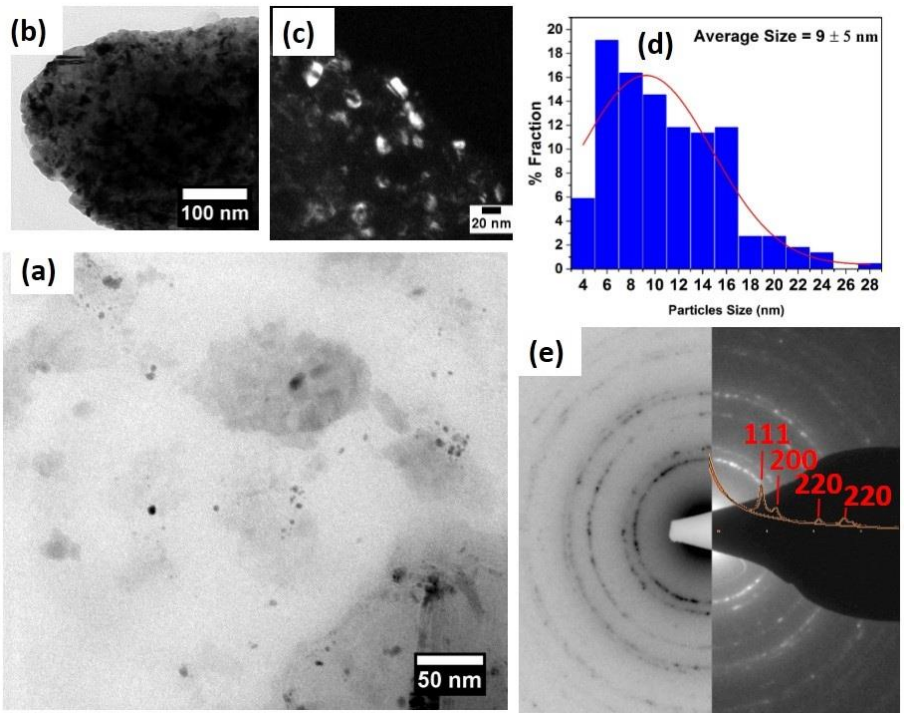

Figure4: (a-b) TEM bright field image of HEAs –NPs ($Cu_{0.2}Ag_{0.2}Au_{0.2}Pt_{0.2}Pd_{0.2}$); **(c)** dark field image of nanoparticles; **(d)** distribution of HEA-NPs; **(c)** selected area diffraction pattern.

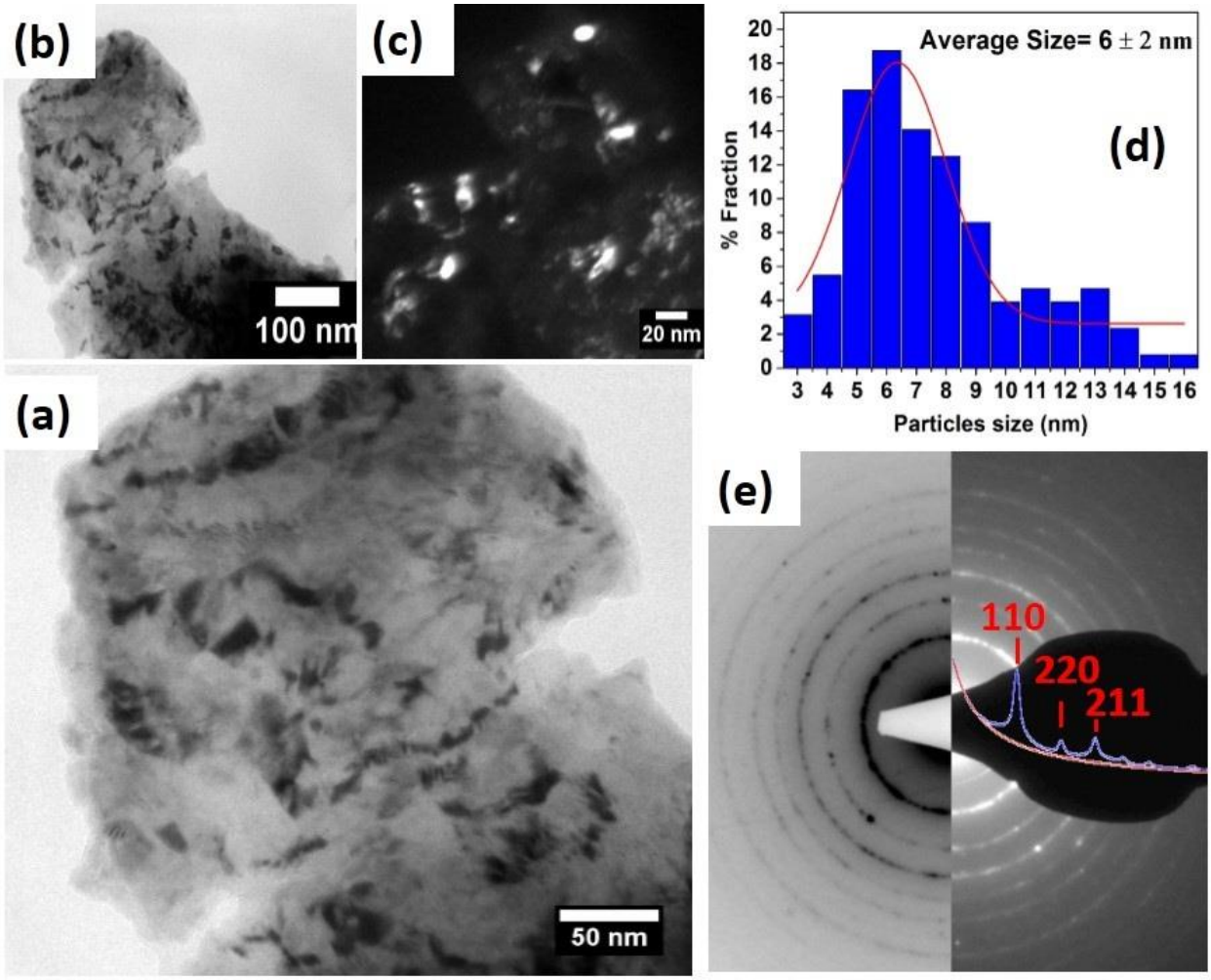

Figure 5: (a-b) TEM bright field image of HEAs –NPs ($Fe_{0.2}Cr_{0.2}Mn_{0.2}V_{0.2}Al_{0.2}$); **(c)** dark field image of nanoparticles; **(d)** size distribution of HEA-NPs; **(e)**selected area diffraction pattern.

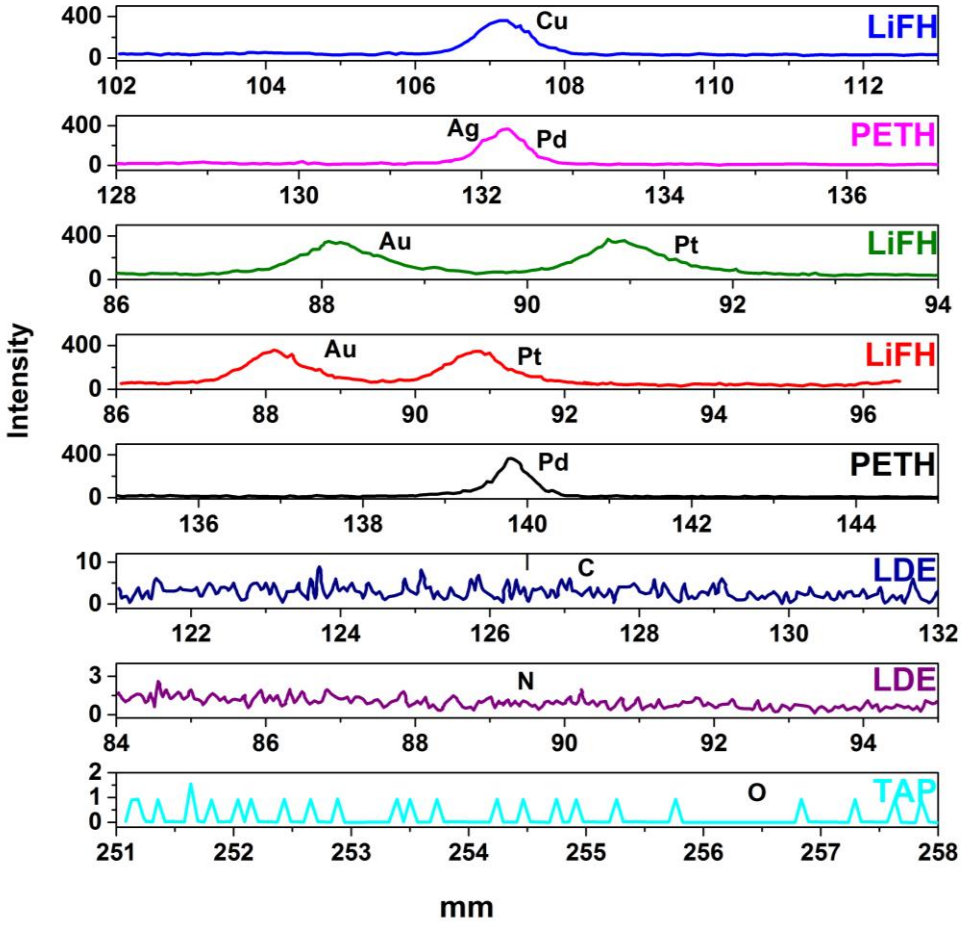

Figure 6: EPMA spectra (WDS) of $Cu_{0.2}Ag_{0.2}Au_{0.2}Pt_{0.2}Pd_{0.2}$ nanoparticles. (Lithium fluoride (LiFH) crystals; Layered dispersion element (LDE); Pentaerythritol (PET); Thallium acid phthalate (TAP))

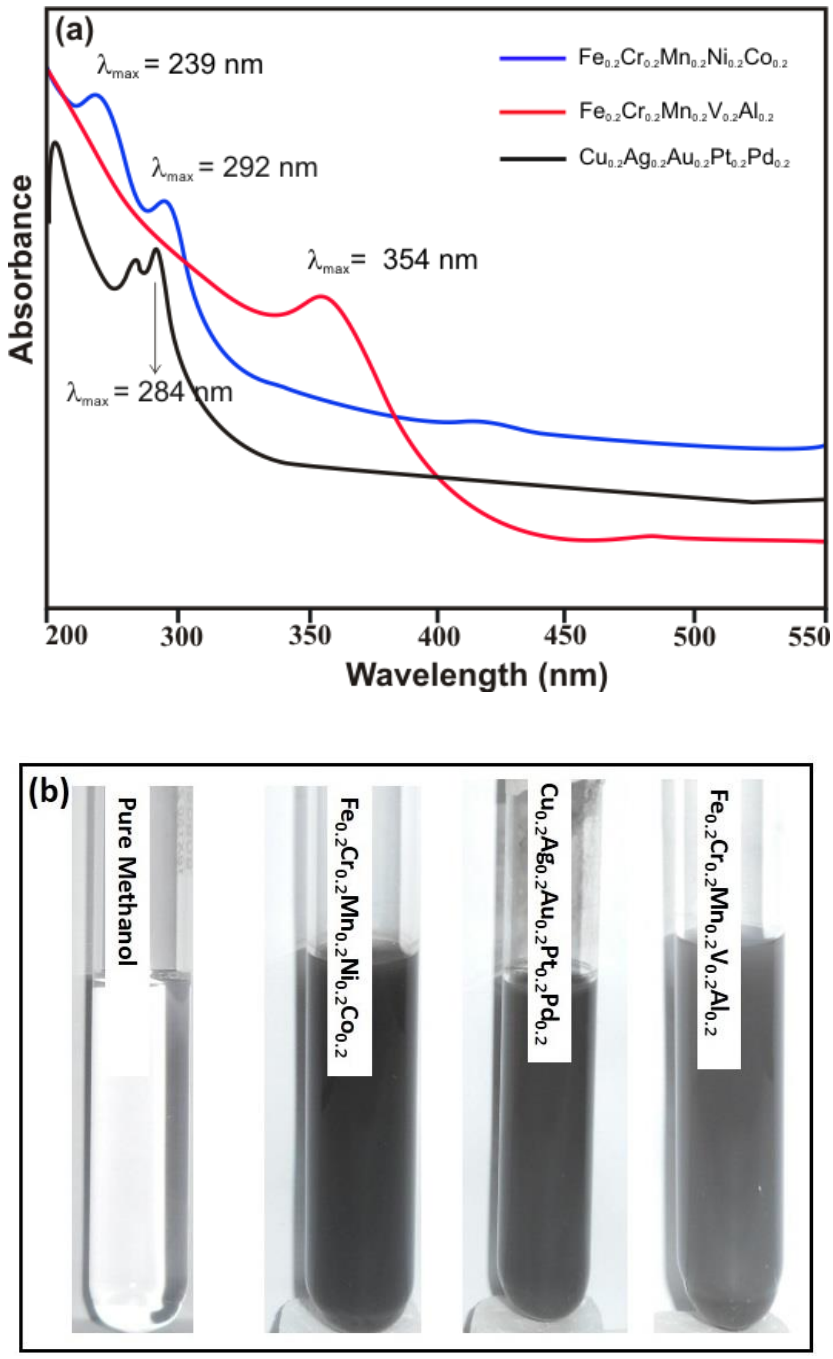

Figure 7: (a)UV-visible spectrum of HEAs-NPs dispersed in pure methanol; **(b)** optical image of after 12 hours of dispersion HEAs-NPs in pure methanol.

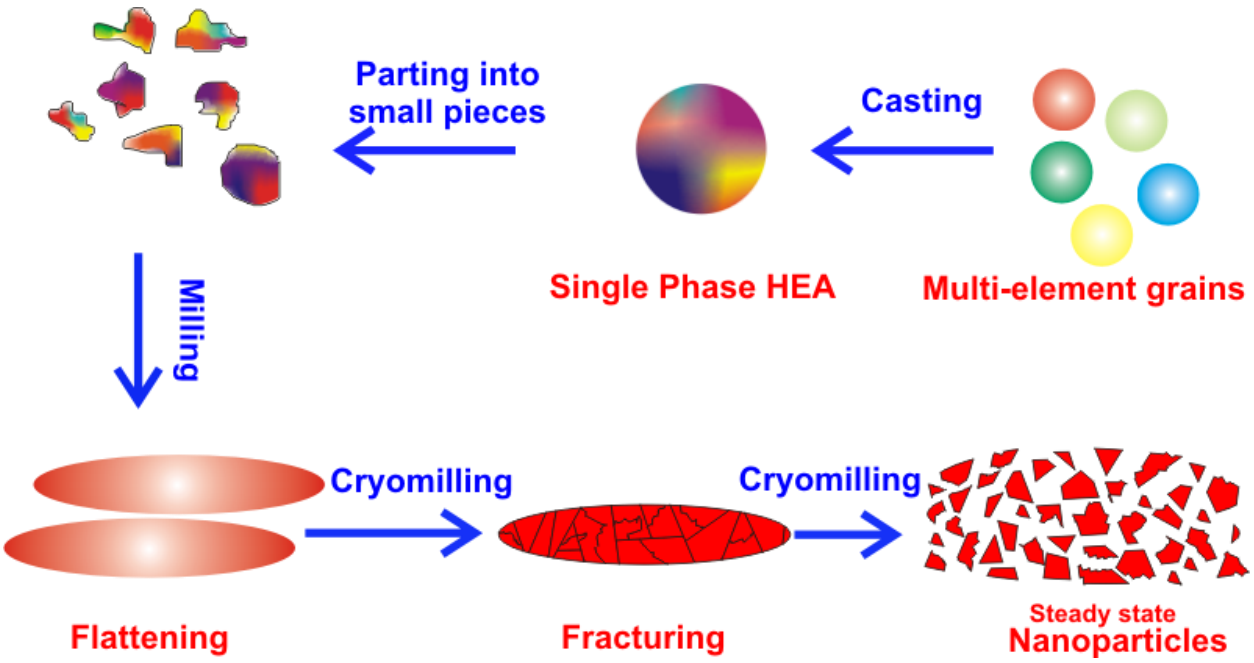

Figure 8: Schematics of HEAs nanoparticles formation process step in cryomilling